Liquid Crystals
Publication details, including instructions for authors and subscription information:
http://www.tandfonline.com/loi/tlct20

Ferroelectric liquid crystalline polymers based on mesogens with halogen-containing terminal groups

Yi-An Sha [a] , Ging-Ho Hsiue [a] , Chih-Ho Chiu [a] , Ru-Jong Jeng [b] & Hsing-Chieh Tai [c]
[a] Department of Chemical Engineering, National Tsing Hua University, Hsinchu, Taiwan 300 ROC
[b] Department of Chemical Engineering, National Chung Hsing University, Taichung, Taiwan 402 ROC
[c] Department of Applied Chemistry, National Chiao Tung University, Hsinchu, Taiwan 300 ROC
Published online: 11 Nov 2010.

LIQUID CRYSTALS, 2003, VOL. 30, NO. 1, 71–80

Ferroelectric liquid crystalline polymers based on mesogens with halogen-containing terminal groups

YI-AN SHA, GING-HO HSIUE*, CHIH-HO CHIU
Department of Chemical Engineering, National Tsing Hua University, Hsinchu, Taiwan 300 ROC

RU-JONG JENG
Department of Chemical Engineering, National Chung Hsing University, Taichung, Taiwan 402 ROC

and HSING-CHIEH TAI
Department of Applied Chemistry, National Chiao Tung University, Hsinchu, Taiwan 300 ROC

(*Received 29 May 2002; accepted 23 August 2002*)

A new series of halogen-containing side chain ferroelectric liquid crystal polymers was synthesized. Mesophases were characterized by differential scanning calorimetry, polarizing optical microscopy, X-ray diffraction and molecular simulation. The behaviour of the liquid crystalline phase was investigated with variation of chiral centres, spacer units and grafted ratios. It was found that the thermal stability and temperature range of the chiral smectic C phase decreased with increasing length of the oligo-oxyethylene spacer, and decreasing mesogenic group content. The bulky substituent attached to the chiral centre reduces molecular packing in smectic liquid crystal phases, which disturbs the orientation of the side chain liquid crystal polymer. Furthermore, the influence of molecular structure on electro-optical properties of FLCPs has been studied by broad band dielectric spectroscopy (from 0.1 to 1×10^6 Hz).

1. Introduction

Ferroelectric liquid crystal polymers (FLCPs) have been investigated extensively in recent decades. FLCPs combine properties such as large spontaneous polarization, memory effect, high mobility, viscous flow, and easy fabrication as thin solid films [1–4]. Despite the fact that FLCPs are inferior to FLCs for fast switching electro-optical (EO) display applications due to their higher viscosity, the aforementioned characteristics make them suitable for electro-optical device applications, such as light valves and memory devices [5, 6].

In general, improvement of the molecular mobility of FLCPs would lower their relaxation time. Four different mechanisms have been proposed for increasing molecular mobility: (i) a longer spacer length that would reduce the interaction between the FLC monomer and polymer backbone [7]; (ii) lateral substitution into the mesogenic group leading to the formation of a less-ordered mesophase [8]; (iii) copolymer and/or (iv) guest-host systems that would exhibit better molecular mobility due to the plasticizer effect [9].

The dielectric properties of FLCPs are closely associated with the reorientation of mesogenic group and with the relaxation (or response) time under an alternating electric field. Zentel *et al.* observed several relaxation processes for FLCPs [10]. Below T_g, two relaxation processes corresponding to reorientation of the dipoles at the mesogenic group centre (β-relaxation), and the spacer group (γ-relaxation) are present. α-Relaxation corresponds to T_g, and the polymer main chain becomes mobile during this transition. δ-Relaxation is the reorientation of the long axis of the side chain group around the polymer backbone. This relaxation can be observed at temperatures higher than T_g for the liquid crystalline polymer. The collective FLC relaxation (Goldstone mode) in the chiral smectic phase has been studied by several investigators [7, 8]. The Goldstone mode appears in the chiral smectic phase, with the fluctuation in the azimuthal orientation of the director. This relaxation mode is an important dielectric characteristic in the chiral smectic phase.

* Author for correspondence; e-mail: ghhsiue@che.nthu.edu.tw

Liquid Crystals ISSN 0267-8292 print/ISSN 1366-5855 online © 2003 Taylor & Francis Ltd
http://www.tandf.co.uk/journals
DOI: 10.1080/0267829021000043349

In our previous work, a series of halogen(F, Cl, or Br)-containing FLCs and FLCPs were synthesized and characterized [11]. Except for the bromine-containing homopolymers PS*n*12Bs100 ($n = 1$, 2 or 3), all the materials exhibited a wide temperature range chiral smectic C phase. It is important to note that bromine-containing liquid crystals do exhibit the chiral smectic C phase. The absence of a chiral smectic C phase for bromine-containing homopolymers may result from repulsion among the more bulky asymmetric chiral centres constrained by polymer chains. It seems to be a reasonable approach to remove the polymer chain constraint, leading to a copolymer system. In this paper, a new series of halogen-containing side chain liquid crystalline polymers and copolymers are described. These liquid crystalline materials consist of halogen-containing chiral moieties, oligo-oxyethylene spacers, and an ester core unit. The influences of the chiral moieties, grafted contents and spacer units on phase formation, thermal properties, conformations, and EO properties are discussed.

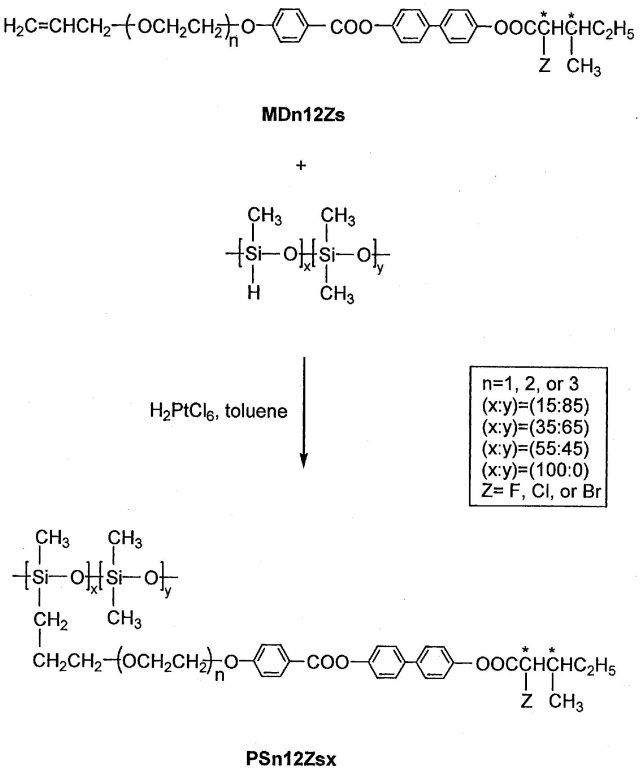

Scheme. Synthesis of polysiloxane series PS*n*12Bs*x* ($n = 1$, 2 or 3; $x = 15$, 35, 55 or 100).

2. Experimental

2.1. *Materials*

Poly[(15 ~ 18%)methylhydrogensiloxane-co-(82 ~ 85%)-dimethylsiloxane] ([η] = 25 ~ 35), poly[(30 ~ 35%)-methylhydrogensiloxane-co-(65 ~ 70%)dimethylsiloxane] ([η] = 25 ~ 30), poly[(50 ~ 55%)methylhydrogensiloxane-co-(45 ~ 50%)dimethylsiloxane] ([η] = 20 ~ 15) and poly-(methylhydrogensiloxane) ([η] = 30) were purchased from United Chemical Technologies, Inc.; methanol was purchased from TEDIA. All the above chemicals were used as received. Toluene was purchased from TEDIA and distilled over sodium under nitrogen using benzophenone as an indicator.

2.2. *Synthesis*

The synthesis and characterization of FLC monomers have been reported previously [10]. The synthesis of the liquid crystalline polysiloxanes is outlined in the scheme. These polysiloxanes were synthesized via a hydrosilation reaction as reported previously [10]. One example, the synthesis procedure for PS312Bs15, is described below.

FLC monomer, MD312Bs (0.5 g, 10 mol % excess versus the Si–H groups present in the polysiloxane), was dissolved in 50 ml of freshly distilled toluene together with appropriate amounts of poly[(15 ~ 18%)methylhydrogensiloxane-co-(82 ~ 85%)dimethylsiloxane]. This solution was heated under reflux under nitrogen. Then hydrogen hexachloroplatinate(IV) hydrate (100 µg) in dry THF was injected by syringe. The solution was heated under reflux under nitrogen for a further 24 h. It was then evaporated under reduced pressure to give a crude yellow viscous fluid. This product was purified by several precipitation with methanol, and dried under vacuum.

2.3. *Characterization*

^{1}H NMR spectra were obtained with a Bruker AM-400 NMR spectrometer. Transition temperatures were determined as the maxima of the endothermic or exothermic peaks obtained from thermal scans using a Seiko SSC 5200 differential scanning calorimeter (DSC). Heating and cooling rates were 10°C min^{-1} in all cases, and the transition temperatures were obtained from the specified first cooling and second heating scans. A Nikon Microphoto-Fx polarizing optical microscope (POM), equipped with a Mettler FP82 hot stage, was used to observe the thermal transitions and anisotropic textures. X-ray diffraction (XRD) measurements were made with a Rigaku R-axis IIC powder diffractometer. A monochromatized X-ray beam from nickel-filtered Cu K_α radiation with a wavelength of 0.15406 nm was used. The X-ray diffractometer was temperature controlled with a tolerance of ± 0.5°C.

2.4. *Simulation*

Molecular dynamics simulations were carried out on a Silicon Graphics Iris O2 workstation. The molecular dynamic trajectories were calculated with the aid of Cerius[2] supplied by Molecular Simulations, Inc.

Initial models were developed from a single macromolecule in vacuum, and were minimized by using steepest descents and conjugated gradients for 1000 steps. The molecular dynamics was performed under a canonical (NVT) ensemble by the Nosé thermal coupling method [12, 13]. The Dreiding II force field was used for the energy calculation [14]. Molecular dynamics were run at 333 K for 1×10^5 ps; ten cycles of molecular dynamics were carried out for each model structure.

2.5. *Dielectric properties*

The dielectric spectroscopy was determined by a Novocontrol GmbH spectrophotometer. Measurements were performed on a Schlimberger SI 1260 impedance/gain-phase analyser (frequency 10^{-1} to 10^6 Hz) with a Quatro temperature controller. The measurement system was fully computer controlled. A nitrogen gas heating system ranging from -100 to 215°C was used; temperatures were adjusted within a tolerance of ± 0.05°C. FLCP samples were sandwiched between two parallel metal electrode plates with a spacer of 50 μm.

3. Results and discussion

3.1. *Synthesis*

Chemical structures of the compounds were identified by ^{1}H NMR spectra. In one example of PS312Bs15, chemical shift appearing at 4.02 ppm could be associated with the $-C\underline{H}Br-$ proton of the chiral centre. On the other hand, the Si–H peak at 4.7 ppm and vinyl protons of the $C\underline{H}_2{=}C\underline{H}-$ group, appearing between 5.23 and 5.90 ppm, vanished after reaction. This confirms the complete reaction between FLC monomers and Si–H groups.

3.2. *Thermal properties*

Phase sequences and corresponding transition temperatures for the FLCPs are shown in table 1. All the FLCPs exhibit a chiral smectic C phase except for the homopolymers PS112Bs100, PS212Bs100, and PS312Bs100. PS112Bs*x* ($x = 15, 35, 55$) show enantiotropic cholesteric (Ch), chiral smectic C (SmC*), and high order smectic (SmX) phases, while PS312Cs100, PS312Fs100, PS312Bs55, and PS212Bs*x* ($x = 15, 35, 55$) exhibit enantiotropic Ch, and SmC* phases. It is important to note that PS312Bs15 and PS312Bs35 copolymers exhibit only the SmC* phase. Homopolymers PS112Bs100, PS212Bs100, and PS312Bs100 show only the Ch phase.

3.3. *Spacer effect*

Series PS*n*12Bs15 ($n = 1$, 2 or 3) was used to investigate the spacer effect on mesophases. PS112Bs15 ($n = 1$) shows enantiotropic Ch, SmC*, and SmX phases whereas PS212Bs15 ($n = 2$) exhibits enantiotropic Ch and SmC* phases. Meanwhile, PS312Bs15 ($n = 3$) exhibits only the SmC* phase. All three compounds reveal wide temperature ranges of the SmC* phase. These temperature ranges were wider than that of FLC monomer MDn12Bs [10]. It is important to note that the temperature range of the SmC* phase was more than 100°C for PS312Bs15. A flexible polysiloxane backbone enhances the decoupling of the motions of the side chain and main chain, which tends to give rise to a better thermal stability of mesophases such as the SmC* phase [15].

The temperature range and thermal stability of the liquid crystal phase were increased with increasing spacer length. The glass transition temperatures (T_g) of these polymers were observed in DSC thermograms; it decreased with increasing spacer repeat units due to the plasticizer effect. The temperature range of Ch phases increased with decreasing spacer length. A shorter spacer increased the molecular interaction of side chain mesogenic groups, and hindering the lateral packing of the SmC* phase.

XRD measurements and POM were used to verify the assignment of the mesophase for these polymers. For PS112Bs15, the POM micrograph reveals a focal-conic texture at 96°C (figure 1). Figure 2 presents temperature-dependent XRD diagrams obtained from a powder sample of PS112Bs15 at 35, 55, 70, 95, 110 and 130°C. Upon further cooling from the cholesteric phase, two sharp reflections at low angle and two broad reflections at wide angle were assigned as the lateral packing and the smectic layer, respectively. This indicates the microscopic

Figure 1. Optical polarizing micrograph of PS112Bs15 revealing SmC* phase at 96°C (800×).

Table 1. Phase transition temperatures for the FLCPs.

Sample	n[a]	x[a]	Z[a]	Heating / Cooling	Phase transitions temperatures/°C[b] (corresponding enthalpy changes/kJ kg^{-1})
PS312Fs100	3	100	F	heating	g 28.6 SmC* 143 (−)[c] Ch 163 (−)[c] I
				cooling	I 153.34 (−)[c] Ch 137.4 (−)[c] SmC* 32.4 g
PS312Cs100	3	100	Cl	heating	g 17 SmC* 131.9 (−)[c] Ch 149.8 (−)[c] I
				cooling	I 145.5 (−)[c] Ch 128.1 (−)[c] SmC* 12 g
PS112Bs15	1	15	Br	heating	g 10.8 SmX 26.6 (1.6) SmC* 104.3 (1.7) Ch 133.3 (0.8) I
				cooling	I 131.5 (0.9) Ch 100.7 (1.3) SmC* 21.6(0.9) SmX 0.5 g
PS112Bs35	1	35	Br	heating	g 12.2 SmX 30.2 (−)[c] SmC* 101.3 (0.9) Ch 131.6 (0.4) I
				cooling	I 128.6 (0.6) Ch 96.9 (0.6) SmC* 26.2 (−)[c] SmX 1.9 g
PS112Bs55	1	55	Br	heating	g 15.8 SmX 35.8 (0.5) SmC* 100.3 (1.9) Ch 129.3 (0.3) I
				cooling	I 127.0 (0.4) Ch 95.3 (1.3) SmC* 30.4 (0.4) SmX 11.8 g
PS112Bs100	1	100	Br	heating	g 16.5 Ch 133.5 (−)[c] I
				cooling	I 127.2 (−)[c] Ch 12.9 g
PS212Bs15	2	15	Br	heating	g −15.2 SmC* 89.3 (1.7) Ch 113.7 (0.8) I
				cooling	I 106.2 (0.7) Ch 79.0 (1.6) SmC* −18.4 g
PS212Bs35	2	35	Br	heating	g −13.3 SmC* 74.1 (−)[c] Ch 86.6 (−)[c] I
				cooling	I 82.1 (0.3) Ch 66.4 (0.1) SmC* −16.8 g
PS212Bs55	2	55	Br	heating	g −12.5 SmC* 68.7 (1.2) Ch 81.2 (0.4) I
				cooling	I 79.4 (0.4) Ch 64.2 (4.6) SmC* −16.4 g
PS212Bs100	2	100	Br	heating	g −8.3 Ch 102.7 (−)[c] I
				cooling	I 97.5 (−)[c] Ch −11.1 g
PS312Bs15	3	15	Br	heating	g −34.6 SmC* 85.1 (1.2) I
				cooling	I 83.8 (1.1) SmC* −40 g
PS312Bs35	3	35	Br	heating	g −20.4 SmC* 83.3 (1.5) I
				cooling	I 82.3 (2.3) SmC* −26.0 g
PS312Bs55	3	55	Br	heating	g −18.2 SmC* 54.7 (1.0) Ch 62.7 (−)[c] I
				cooling	I 58.5 (−)[c] Ch 52.3 (−)[c] SmC* −21.8 g
PS312Bs100	3	100	Br	heating	[d]
				cooling	I 105.4 (0.6) Ch 7.4 (0.7)

[a] n, x, Z according to the scheme.
[b] I = isotropic phase; Ch = cholesteric phase; SmC* = chiral smectic C phase; SmX = unidentified smectic phase; g = glassy state.
[c] Enthalpies were too small to be evaluated.
[d] No liquid crystalline phase was observed.

phase separated between the polymer backbone and the LC domain [16]. Curve B exhibits a diffuse reflection at 4.95 Å and a very weak reflection at 39.49 Å, which correspond to the smectic layers. Moreover, the *d*-spacing of the first order reflection falls from 39.49 to 35.73 Å (curve B to curve E) as the temperature of measurement decreases from 110 to 55°C. The temperature dependence of the layer spacing for PS*n*12Bs15 is presented in figure 3(*a*); the *d*-spacing decreases as the temperature decreases. Judging from the results of POM micrographs and XRD measurements, the formation of a tilted SmC* phase is confirmed. On the other hand, the *d*-spacing increases with increasing spacer length. This is due to the increase of molecular length of the side chain group.

Similar phase behaviour was found in the PS*n*12Bs35 and PS*n*12Bs55 series ($n = 1$, 2 or 3). All of the FLCPs exhibit the SmC* phase. The SmC* phase temperature range and thermal stability are increased with increasing spacer length due to increasing flexibility of the side chain group; temperature-dependent *d*-spacings are presented in figure 3(*b*) and 3(*c*).

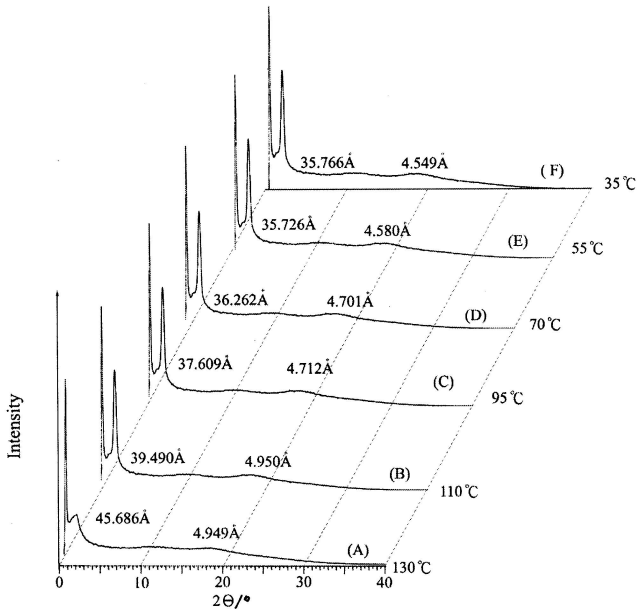

Figure 2. X-ray diffraction measurements for PS112Bs15.

3.4. *Effect of grafted contents and chiral centres*

As an example, PS312Bs*x* is used to describe the effect of grafted content on thermal properties. T_g increases with increasing grafted content (from −40 to 7.4°C) due to the increase in rotation hindrance by the side chain mesogenic group. The PS312Bs15, PS312Bs35, and PS312Bs55 samples exhibit wide SmC* temperature ranges, including room temperature. Yet PS312Bs100 shows only the cholesteric phase. The SmC* temperature range narrows (from 123.8 to 74.2°C) as the grafted content increases. This suggests that the decrease of the mesogenic group content raises the thermal stability of the SmC* phase. In addition, the phase transition temperatures of copolymers are lower than those of homopolymers because of the dilution of mesogenic groups on the polymer backbones [17].

As mentioned above, halogen(F, Cl and Br)-containing FLCP homopolymers were previously reported by us [10]. The fluorine- and chlorine-containing homopolymers show the SmC* mesophase. However, the bromine-containing PS*n*12Bs100 ($n = 1$, 2, or 3) homopolymers show no smectic mesophase. Furthermore, the FLC monomer MD*n*12Bs ($n = 1$, 2 or 3) exhibits a wide temperature range (about 80°C) SmC* mesophase. Based on the above, the use of polysiloxane as the polymer backone for FLCPs would normally increase thermal stability and widen mesomorphic temperature range. However, there is an exception; as shown previously, the bromine-containing polysiloxane homopolymer shows no SmC* phase. This is possibly because the bulky chiral centre disturbs lateral packing of the mesogenic group and hence lowers the thermal stability of a chiral

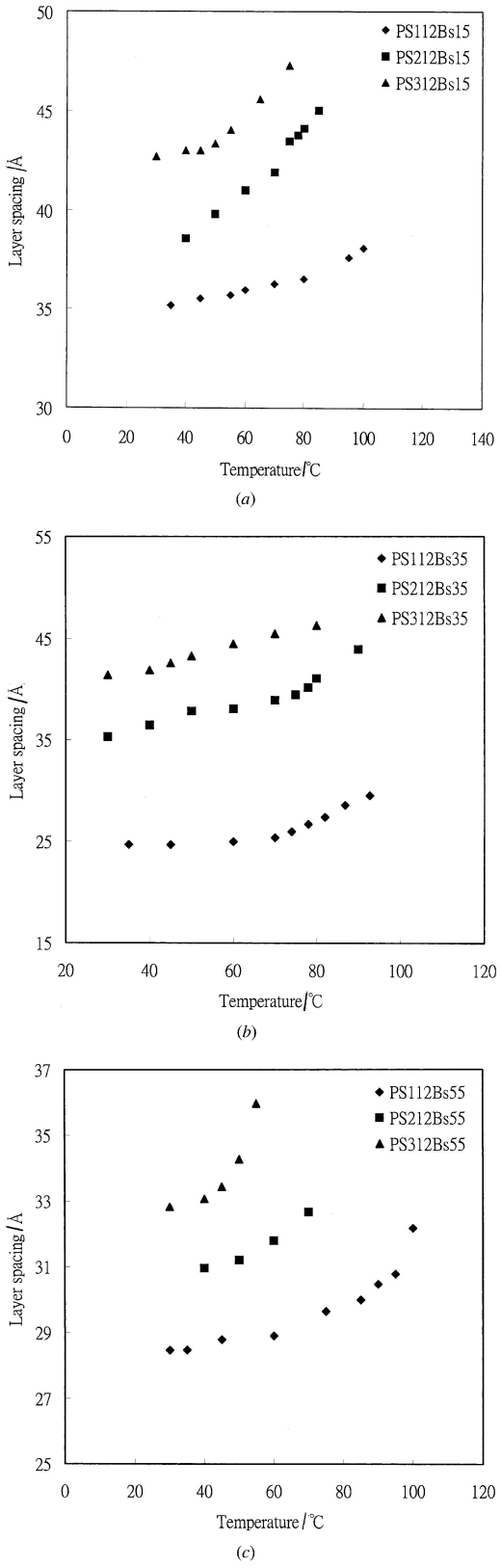

Figure 3. Layer spacing as a function of temperature in the SmC* phase of samples (*a*) PS*n*12Bs15, (*b*) PS*n*15Bs35 and (*c*) PS*n*12Bs55.

smectic phase under the constraint of polymer chains. The size of molecules containing F, Cl and Br are shown in table 2 [18].

3.5. *Molecular simulation*

Following the preliminary studies of thermal properties/molecular structure relationships, molecular simulation was performed on the equilibrated structures of the FLCPs. In this section, two extreme models of PS112Bs100 and PS112Bs15, with the respective highest and lowest molecular interactions, are discussed.

Modelling of PS112Bs100 and PS112Bs15 was carried out via single-macromolecule species in vacuum, to investigate the relaxed configuration of the FLCPs. Initially, minimization cycles using steepest descents and conjugated gradients for 1000 steps were performed. The lowest energy configurations are shown in figure 4; a fan-shaped structure for PS112Bs100 was found. This is due to the repulsive force between side chain mesogenic groups. Moreover, PS112Bs15 exhibits a fully extended smectic structure.

The molecular dynamics was run under a canonical (NVT) ensemble by the Nosé thermal coupling method at 333 K for 1×10^5 ps; ten cycles of molecular dynamics were carried out on each model structure. Figure 5 shows the equilibrated structures of PS112Bs100 and PS112Bs15. PS112Bs100 presents a helical configuration corresponding to the cholesteric phase, whereas PS112Bs15 still exhibits the smectic phase as mentioned in the discussion of thermal properties. This further corroborates results described in the previous section.

3.6. *Dielectric properties of PS312Fs100, PS312Cs100, and PS312Bs100*

Dielectric constant ε' versus temperature and frequency for PS312Fs100 is shown in figure 6(*a*). For both PS312Fs100 and PS312Cs100, the dielectric constant increases with increasing temperature in the SmC* phase due to the presence of the Goldstone mode. With the electro-induced phase transition effect, the Goldstone mode was also observed for PS312Bs100 in the Ch phase, figure 6(*b*). The Goldstone mode results from the large fluctuation of the spontaneous polarization director of the tilt vector at constant tilt angle under an alternating electric field [19–21]. With the decreasing viscosity and increasing fluctuation, the dielectric constant increases. Moreover, as the temperature increased, the molecular tilt angle decreased in the SmC* phase; this is because the rotational freedom increased somewhat on decreasing the steric hindrance. In addition, the dielectric constant increased with increasing temperature at low frequency (below 1 kHz) due to the large fluctuation of the Goldstone mode. This Goldstone mode

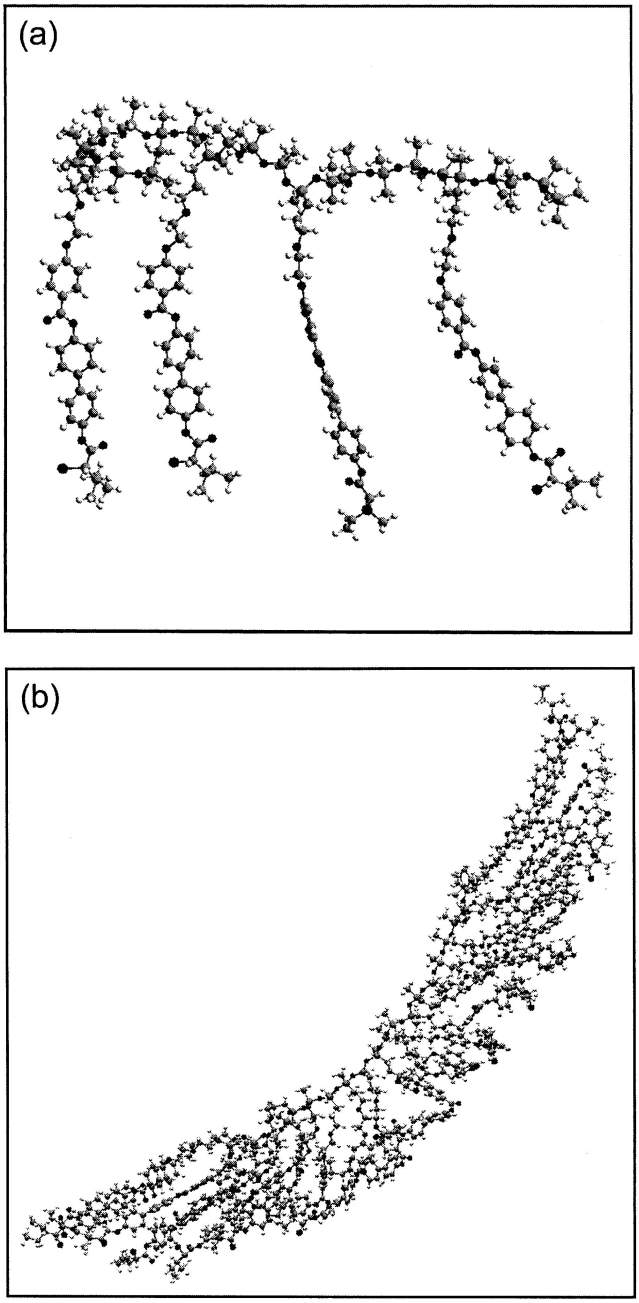

Figure 4. Lowest energy configurations of (*a*) PS112Bs15 and (*b*) PS112Bs100.

Table 2. Molecular sizes of FLCPs containing F, Cl and Br.

Substitution	Size/Å
F	1.47
Cl	1.75
Br	1.85

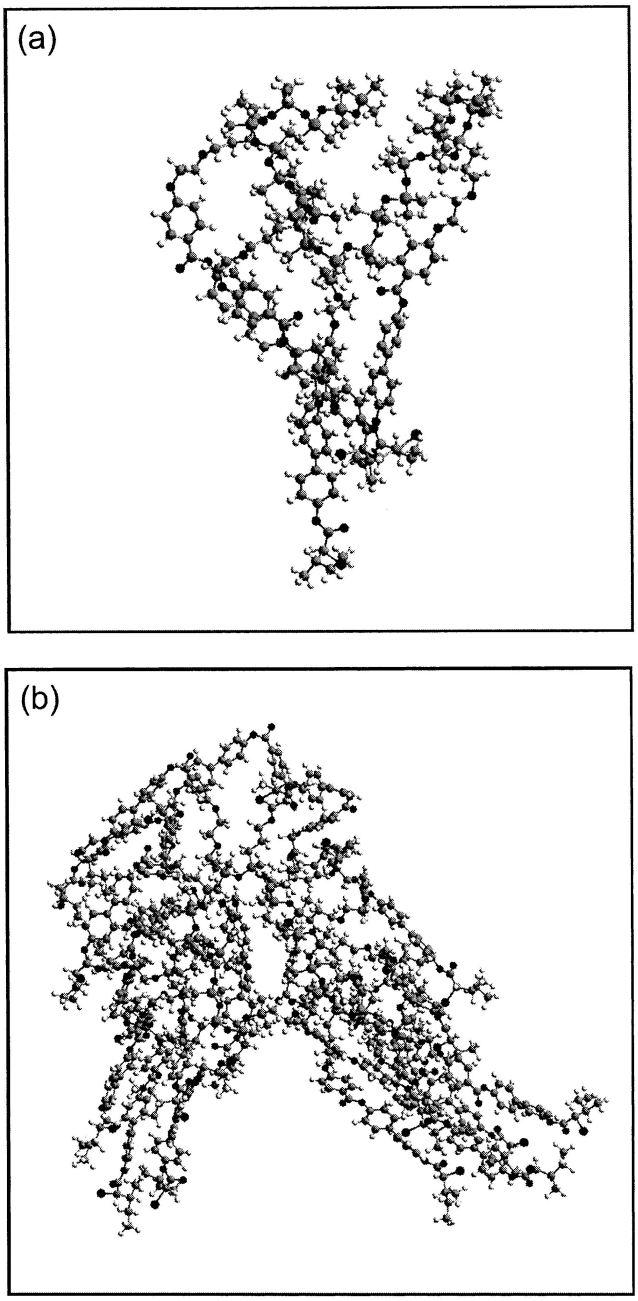

Figure 5. Equilibrated structures of (*a*) PS112Bs15 and (*b*) PS112Bs100 at 333 K.

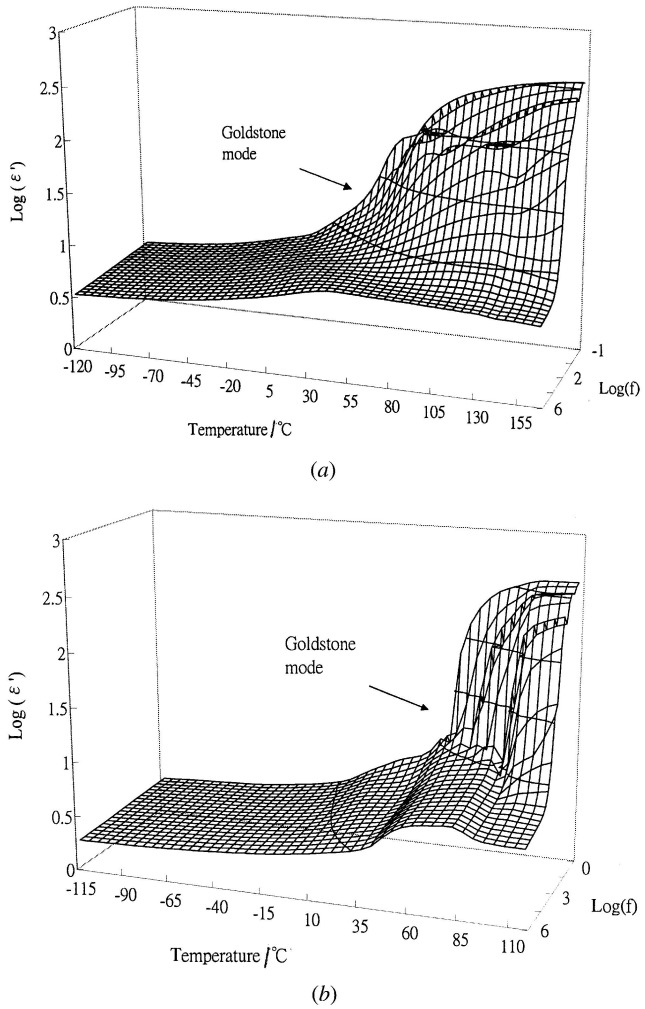

Figure 6. Dielectric constant ε' versus temperature and frequency for (*a*) PS312Fs100 and (*b*) PS312Bs100.

requires a longer relaxation time for FLCPs. Above the SmC*–Ch phase transition temperature, the dielectric constant increased as the temperature increased, at low frequency (below 1 Hz), due to the ionic conductivity effect of the samples. The relaxation intensity of the Goldstone mode was increased and shifted to a higher frequency range, due to a loosening of the dense packing of the highly tilted smectic phase, and increasing mobility of the side chain groups. The increase of the relaxation intensity and frequency of the Goldstone mode is important in the electro-optical application of the FLCPs [7–10]. A bulky terminal group loosens the dense packing and increases the mobility of the tilted smectic phase under alternative electric fields for PS312Bs100.

Dielectric loss ε'' as a function of temperature and frequency for PS312Fs100 and PS312Bs100 is shown in figures 7 (*a*) and 7 (*b*), respectively. At a higher temperature range, the presence of the Goldstone mode in all the samples leads to an increase of the dielectric loss. Molecular relaxations of the PS312Fs100, PS312Cs100, and PS312Bs100 samples were also observed (see table 3). The α-relaxation was associated with the glass transition T_g. This process is attributed to molecular motion involving the polymer main chain and side chain group. The α-relaxation was shifted to a higher temperature with increasing frequency; it was absorbed by the Goldstone mode as the temperature further increased.

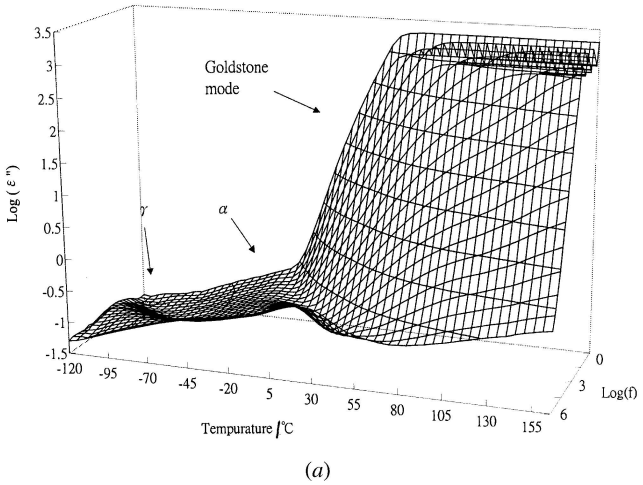

(*a*)

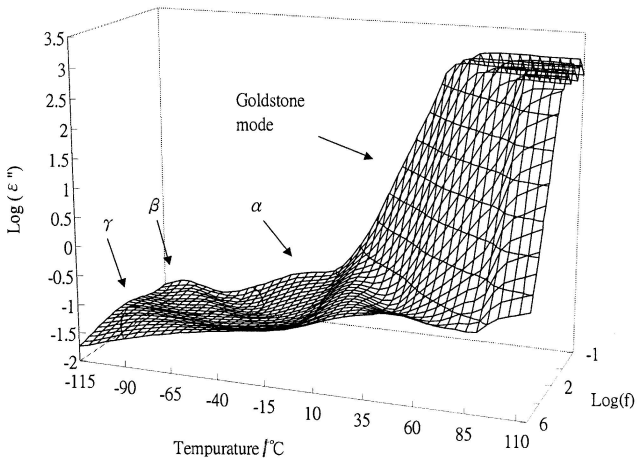

(*b*)

Figure 7. Dielectric loss ε'' versus temperature and frequency for (*a*) PS312Fs100 and (*b*) PS312Bs100.

Table 3. Activation energies (kJ mol^{-1}) of the molecular relaxations for PS312Fs100, Ps312Cs100 and PS312Bs100.

	Relaxation		
Sample	α	β	γ
PS312Fs100	219.56[a]–363.06[b]	—[c]	37.74
PS312Cs100	—[c]	—[c]	38.02
PS312Bs100	292.24[a]–369.36[b]	—[c]	38.17

[a] The data were calculated at 103 Hz.
[b] The data were calculated at 105 Hz.
[c] The relaxations were too weak or overlap with another relaxation.

The β-relaxation usually corresponds to the reorientation of the mesogenic group of the FLCPs. Due to the highly rigid mesogenic group and overlapping of the γ-relaxation at lower temperatures, no β-relaxation was found for FLCPs. In these polymers, the γ-relaxation, which corresponds to the reorientation of the spacer group of the FLCPs, was observed. In general, a δ-relaxation is present at temperatures higher than for the α-relaxation; this corresponds to the rotation of side chain groups around the polymer backbone. However, no δ-relaxation was observed in these polymers due to the overlapping of the Goldstone mode.

Analysis of the dielectric behaviour of the FLCPs by a Cole–Cole plot (ε' versus ε'') provides valuable information about the dielectric relaxation process. The Cole–Cole plot of the γ-relaxation at various temperatures for PS312Fs100 is shown in figure 8. The relaxation strength increased with increasing temperatures. In addition, the centre of the circle was shifted to larger ε' values at higher temperatures. However, no Cole–Cole plot could be obtained for β- and δ-relaxations because the β-relaxation was too weak, and the δ-relaxation was overlapped by Goldstone mode. The shape of the Cole–Cole plot can be analysed using the Havriliak–Negami relationship, equation (1):

$$\varepsilon(\omega) = \varepsilon' - \mathrm{i}\varepsilon'' = \varepsilon_\infty + \frac{\Delta\varepsilon}{(1 + \mathrm{i}\omega\tau)^{\alpha',\beta'}} \qquad (1)$$

where ε_∞ is the value of ε' at infinite frequency. $\Delta\varepsilon$ is the difference between ε' at the 0 Hz and at infinite frequency; ω, τ, α', and β' are frequency, relaxation time, width parameter, and asymmetry parameter, respectively.

From the curve of the Cole–Cole plot, the dielectric relaxation intensity $\Delta\varepsilon$ at various temperatures was obtained. Figure 9 shows the γ-relaxation intensity as a function of temperature, indicating that the relaxation intensity increased with decreasing molecular size of the chiral centre. A decrease in the size of the chiral centre favours a better reorientation of the molecular segments toward an alternating electric field. The relaxation

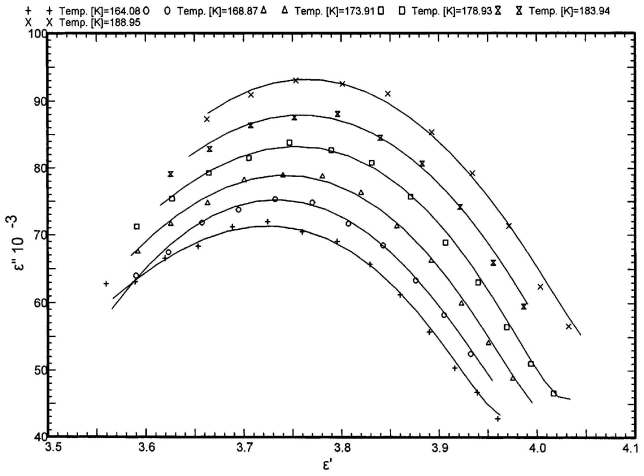

Figure 8. Cole–Cole plot of the γ-relaxation at various temperatures for PS312Fs100.

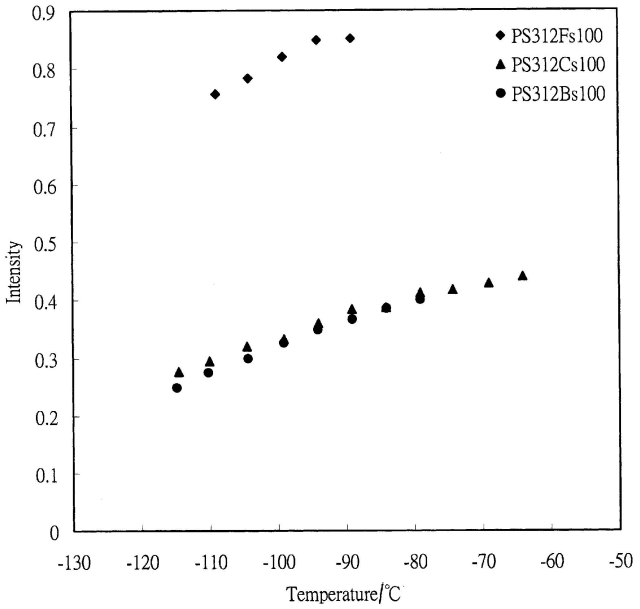

Figure 9. γ-Relaxation intensity as a function of temperature for PS312Fs100, PS312Cs100 and PS312Bs100.

intensity also decreases with increasing temperature; this is because the higher thermal energy results in the mobility of the dipoles toward the alternating electric field.

Except for the α-relaxation, the relaxation activation energies are obtained using the Arrhenius equation. The α-relaxation frequency ranged from 10^3 to 10^5 Hz. A non-linear curve of the α-relaxation can be fitted with the Williams–Landel–Ferry (WLF) equation [22], indicating that it can be identified as the glass transition [23]. The activation energies of the relaxations are summarized in table 3. Activation energy indicates the presence of molecular interaction; a chiral centre with a smaller molecular size would lower the activation energy of the molecular motions contributing to the α- and γ-relaxations, and thus favours a better reorientation of the molecular segments toward the alternating electric field.

4. Conclusion

In this work, a new series of ferroelectric liquid crystal polymers containing chiral centres attached to halogens, oligooxyethylene spacers, and a three-ring aromatic ester core unit have been developed. Except for the homopolymers, all of the copolymers exhibit the SmC* phase. This is because the bulky substituent on the chiral centre disturbs the orientation of the side chain liquid crystal homopolymer. The dilution of mesogenic groups in an FLC copolymer results in wide temperature range of SmC* phases (about 120°C). An increase in the number of oxyethylene spacer units favours the decrease of clearing and phase transition temperatures; the SmC* phase range narrows as the grafted content increases.

The dielectric properties of a series of FLCPs with different halogenated chiral centres were investigated in this work. The collective and molecular relaxation of these FLCPs were also observed. The dielectric constant was markedly enhanced because of the occurrence of the Goldstone mode in the SmC* phase. The Goldstone mode appears in the Ch phase for homopolymers PS*n*12Bs ($n = 1$, 2 and 3) due to the electro-induced phase transition effect. For PS312Bs, bulky terminal groups loosen the dense packing and increase the mobility of the tilted smectic phase under an alternating electron field. Furthermore, a decrease in the size of the chiral centre results in an increase in the relaxation intensity and decreased activation energy.

The authors thank the National Science Council of the Republic of China for financial support for this work (NSC89-2216-E-007-049-).

References

[1] Clark, N. A., and Lagerwall, S. T., 1980, *Appl. Phys. Lett*., **36,** 899.
[2] Zental, R., Reckert, G., and Reck, B., 1987, *Liq. Cryst*., **2,** 83.
[3] Parmar, D. S., Clark, N. A., Keller, P., Walba, D. M., and Wand, M. D., 1990, *J. Phys. Paris*., **51,** 355.
[4] Dumon, M., Nguyen, H. T., Mauzac, M., Destrade, C., and Gasparoux, H., 1991 *Liq. Cryst*., **10,** 475.
[5] Nakamura, K., Nanataki, H., and Arimoto, M., 1990, *J. appl. Phys*., **67,** 996.
[6] Yuasa, K., Uchida, S., Skuya, T., Hashimoto, K., and Kawasai, K., 1991 *Ferroelectrics*, **122,** 53.
[7] Hsiue, G. H., Lee, R. H., and Hwang, J. C., 1996, *Polymer*, **37,** 1095.
[8] Hsiue, G. H., Lee, R. H., Jeng, R. J., and Chang, C. S., 1996, *J. Polym. Sci. B*, **34,** 555.
[9] Hsiue, G. H., Lee, R. H., and Jeng, R. J., 1997, *Polymer*, **38,** 887.
[10] Zentel, R., Strobl, G. R., and Ringsdorf, H., 1985, *Macromolecules*, **18,** 960.
[11] Hsiue, G. H., Sha, Y. A., Hsieh, S. R., Jeng, R. J., and Kuo, W. J., 2001, *Liq. Cryst*., **28,** 365.
[12] Nosé, S., 1984, *J. chem. Phys*., **81,** 511.
[13] Nosé, S., 1984, *Mol. Phys*., **52,** 255.
[14] Mayo, S. L., Olafson, B. D., and Goddard, W. A., 1990, *J. phys. Chem*., **94,** 8897.
[15] Hsiue, G. H., and Chen, J. H., 1995, *Macromolecules*, **28,** 4366.
[16] Hsiue, G. H., Sha, Y. A., and Jeng, R. J., 2001, *Macromol. Chem. Phys*., **202,** 287.
[17] Hardouin, F., Sigaud, G., Keller, P., Richard, H., Nguyen, H. T., Mauzac, M., and Achard, M. F., 1989, *Liq. Cryst*., **5,** 463.

[18] Collings, P. J., and Hird, M., 1997, *Introduction to Liquid Crystals* (London: Taylor & Francis), p. 71.
[19] Vallerien, S. U., Kremer, F., Kapitza, H., Zentel, R., and Fischer, E. W., 1991, *Ferroelectrics*, **113,** 231.
[20] Vallerien, S. U., Zentel, R., Kremer, F., Kapitza, H., and Fischer, E. W., 1989, *Makromol. Chem. rapid Commun.*, **10,** 333.
[21] Vallerien, S. U., Kremer, F., Scherowsky, G., Schiwa, A., Kuhnpast, K., and Fischer, E. W., 1990, *Liq. Cryst.*, **8,** 719.
[22] Sperling, L. H., 1992, *Introduction to Physical Polymer Science* (Singapore: John Wiley), p. 337.
[23] Malmstrom, E., Liu, F., Boyd, R. H., Hult, A., and Gedde, U. W., 1994, *Polym. Bull.*, **32,** 679.